Exploring the Effect of Pendent Side Chain Length on the Structural and Mechanical Properties of Hydrated Perfluorosulfonic Acid Polymer Membranes by Molecular Dynamics Simulation

An-Tsung Kuo[1,2], Kotono Takeuchi[2], Atsushi Tanaka[1], Shingo Urata[1], Susumu Okazaki[2†], and Wataru Shinoda[2*]

[1]Innovative Technology Research Center, Asahi Glass Co., Ltd., Kanagawa 221-8755, Japan

[2]Department of Materials Chemistry, Nagoya University, Nagoya 464-8603, Japan

†Corresponding author. Tel: (+) 81-52-789-5829. Fax: (+) 81-52-789-5118.

Email: okazaki@chembio.nagoya-u.ac.jp

*Corresponding author. Tel: (+) 81-52-789-5288. Fax: (+) 81-52-789-5118.

Email: w.shinoda@chembio.nagoya-u.ac.jp

ABSTRACT

The side chain (SC) length of perfluorosulfonic acid (PFSA) reportedly influences the proton conductivity and mechanical strength of the membranes in the application of proton exchange membrane. Here, we conducted a series of molecular dynamics simulations to explore the effect of SC length on the morphology and mechanical properties of the PFSA membrane. The results of these simulations pointed to the stronger aggregation of the aqueous domain in the longer SC membranes. This leads to the swollen network structure of the aqueous domains at high water contents, rather than the tortuous layer structure observed in the shorter SC membrane. Furthermore, the mechanical simulation found that the longer SC membranes possessed lower and higher mechanical strengths than the shorter SC membranes at lower and higher water contents, respectively, resulting from the lower ionic strength and larger polymer domains. These findings will be useful for designing new materials for fuel cell applications.

KEYWORDS

Molecular dynamics simulation; perfluorosulfonic acid; side chain; morphology; mechanical deformation

1. INTRODUCTION

Proton exchange membrane fuel cells (PEMFCs) are a highly efficient and green alternative power source [1, 2]. Currently, most PEMFCs use perfluorosulfonic acid (PFSA) ionomers as proton exchange membranes due to their high proton conductivity and high mechanical stability. Flemion® (Asahi Glass Co. Ltd.), Nafion® (DuPont/Chemours), Aciplex® (Asahi Kasei Corp.), and Aquivion® (Solvay) are the most common commercial PFSA membranes. The chemical structure of PFSA consists of a hydrophobic polytetrafluoroethylene (PTFE) backbone with hydrophilic pendent side chains terminated by sulfonic acid groups (Fig. 1). This structural characteristic causes micro-phase separation between the hydrophobic and hydrophilic domains in hydrated PFSA membranes and contributes to its high proton conductivity and mechanical stability [1, 2].

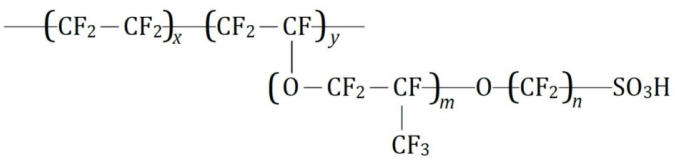

Figure 1. Chemical structure of perfluorosulfonic acid ionomers.

Since proton conductivity is directly influenced by the morphology of the hydrated PFSA membrane, many morphological models have been proposed to describe the water swelling behavior and proton transport mechanism [2-8]. The first such model, the cluster-network model, described the membrane involving spherical domains of a water-rich sulfonic acid phase connected by narrow channels [3, 4]. A subsequent fibrillar structure model suggested that the membrane consisted of elongated polymeric aggregates with cylindrical or ribbon-like shapes surrounded by ionic groups and a water continuum [5, 6]. A parallel cylinder model, in contrast, described the membrane as a locally aligned polymer

matrix, in which parallel cylindrical ionic water channels were embedded [7]. Considerable experimental evidence in favor of the locally flat interfaces (film-like) model has been recently reported by Kreuer and Portale [8]. In addition to these static morphology models, the morphological variation of the membrane under uniaxial stretching has been studied [9-15]. The ionomer backbone and ionic channel were found to have preferred orientations in the direction of stretching, and their alignments increased upon membrane stretching [9, 10, 12-15].

A number of computer simulations of model PFSA systems have been carried out to understand the membrane structure and function at the molecular level [16-18]. *Ab initio* calculations were used to probe the role of the side chains (SCs) of PFSA in proton transfer [19, 20]. Molecular dynamics (MD) simulations were performed to explore various characteristics of the PFSA membranes, including structural and transport properties [21-31], membrane morphology [32-34], gas[35] and water[36, 37] adsorption and permeation, and mechanical deformation [38-42], Multistate empirical valence bond (MS-EVB) methods were adopted to explore the mechanism of proton hopping in water [43-49], Moreover, coarse-grained (CG) simulations were employed to investigate the mesoscale morphology and mechanical properties of the membranes [50-58].

Since the short SC PFSA has been reported to possess better proton conductivity and mechanical properties than long SC PFSA experimentally [59-62], several studies have used MD simulation to explore the effect of SC length on the structural and dynamics properties at the molecular level [26, 63, 64]. Cui *et al.*[63] employed a united-atom MD simulation on the PFSA membrane with different SC length and found that the short SC PFSA membrane (m = 0, n = 2, see Fig. 1) produced a more dispersed cluster distribution at low hydration levels and possessed higher hydronium ion diffusivity than the long SC PFSA membrane (m = 1, n = 2, see Fig. 1). Sunda and Venkatnathan compared the different SC length of PFSA with an

all-atom MD (AA-MD) simulation [64]. They concluded that an extra ether oxygen atom in the long pendent SC of PFSA imparted extra flexibility to the sulfonate group, allowing it to move toward the hydrophilic region and forming a hydrosphere region at high water content. Furthermore, Brandell *et al*.[26] suggested that PFSA with m = 1 and n = 2 (see Fig. 1) can form the hydrated membrane with an optimal water-channel network connectivity.

Although MD studies are somewhat contradictory to experiments in proton conduction due to the simplified molecular model, the MD studies have effectively provided valuable information regarding structural properties of the membranes at the molecular level as mentioned above. However, the role of the secondary ether oxygen has not yet been fully discussed. Also, the effect of SC length on mechanical strength and deformation has not been studied so far. Therefore, in this study, we conducted a series of AA-MD simulations to explore the effect of SC length (secondary ether oxygen) on the morphological and mechanical properties of hydrated PFSA membranes at different water contents. The variation of membrane structure under uniaxial stretching was also investigated. To do so, we modeled three PFSA membranes with m = 0 (short side chain, SSC), 1 (medium side chain, MSC), and 2 (long side chain, LSC) in this study.

The paper is arranged into four Sections. In Section 2, details of molecular modeling and analyses methods, such as radial distribution functions, structure factor, surface area, and order parameter are explained. Then, Section 3 describes computational results on membrane morphology and mechanical properties evaluated from stress-strain curves in uniaxial stretching. In both cases, we especially focus on the effects of the SC length. Eventually, we would summarize some concluding remarks in Section 4.

2. SIMULATION METHODS

2.1. Simulation details

In this study, we examined four PFSA ionomers with different pendent SC lengths (m = 0, 1, and 2, see Fig. 1). The chemical structure and equivalent weights (EW) of the model PFSA ionomers are listed in Table 1. All the PFSA ionomers had 10 repeat units for which n = 2 in the SCs (see Fig. 1). Three of them had 16 (x = 7, y = 1) CF_2 groups in the main chain of the repeat units. The EW of the PFSA ionomers were 978 (m = 0, SSC), 1144 (m = 1, MSC), and 1310 (m = 2, LSC), respectively. The other PFSA ionomer (LSCS) had 10 (x = 4, y = 1) CF_2 groups in the main chains of the repeat unit for which m = 2 in the SC. The EW was 1010. The sulfonic acid groups in the pendent SCs were assumed to be fully ionized to H^+ and SO_3^- at all hydration levels, and the resulting protons combined with water to form hydronium ions (H_3O^+). We constructed PFSA membranes consisting of 200 polymer chains with six different hydration levels (λ = 3, 6, 9, 12, 15, and 20, where $\lambda = (H_2O, H_3O^+)/SO_3^-$). Packmol software was used to generate initial configurations by randomly placing molecules in a cubic box with side lengths of 40 nm [65]. AA-MD simulations were carried out using the Gromacs package, version 5.04 [66, 67]. The modified DREIDING force field by Mabuchi and Tokumasu [31] was adopted for the PFSA ionomers, while the F3C water model [68] and the classical hydronium model [21] were applied for the water molecules and hydronium ions, respectively. The Nosé–Hoover thermostat [69] and Parrinello–Rahman barostat [70, 71] were employed to control the temperature and pressure, respectively. Relaxation times of thermostat and barostat are set to 0.5 ps and 5 ps, respectively. Long-range electrostatic interactions were calculated using the particle-mesh Ewald (PME) method [72], and Lennard–Jones (LJ) pair interactions were evaluated within a cutoff distance of 1.5 nm without a truncation shift function. Time step of 1 fs was used in all MD simulations. Each system was thermalized using the annealing procedure proposed by

Mabuchi and Tokumasu [31], and an equilibrating MD simulation was then conducted for 300 ns at T = 300 K and P = 1 bar. After the equilibrium MD simulation, the final configuration was adopted for mechanical deformation of the membrane. Uniaxial deformation was applied gradually in the z-direction at a constant rate of 0.1 ns^{-1} (1.2–1.5 m/s depending on water content and pendent SC length) up to a strain of 200% at T = 300 K. During the deformation, the pressures in the x- and y-directions were controlled at 1 bar, causing lateral contraction of the simulation box, while the pressure in the z-direction varied according to the applied strain and was monitored to calculate the stress of the membrane. The complete details have been reported in our previous studies [34, 42].

Table 1. Chemical structure and equivalent weights (*EW*) of model PFSA ionomers

	x	*y*	*m*	*n*	*EW*	*IEC**
SSC	7	1	0	2	978	1.02
MSC	7	1	1	2	1144	0.87
LSC	7	1	2	2	1310	0.76
LSCS	4	1	2	2	1010	0.99

**IEC*: Ion-exchange capacity, $IEC = 1000/EW$ (meq/g)

2.2. Simulation analysis

2.2.1 Volume and surface area

To describe the distribution of water within the hydrated membrane, the ratio of the interfacial area (SA) at the water-polymer boundary to the total volume (TV) of the membrane was computed. We used the fast double cubic lattice method [73] to calculate the solvent-accessible surface area of the polymer exposed to the aqueous phase as the interfacial area. In the calculation, a spherical probe with a radius of 0.14 nm was adopted.

2.2.2 Radial distribution function

The local structure of the membrane was examined using radial distribution functions (RDFs),

$$g_{A-B}(r) = \left(\frac{dn_B}{4\pi r^2 dr} \right) \Big/ \left(\frac{N_B}{V} \right), \qquad (1)$$

where n_B is the number of B particles in a *dr*-thick spherical shell located at a distance *r* from particle A; N_B is the total number of B particles in the system; and *V* is the volume of the system.

2.2.3 Structure factor

To probe the morphology of hydrated PFSA membranes, we used the Cromer–Mann relation to determine X-ray scattering intensities of the membranes. The structure factor was computed by:

$$\mathbf{F}(\mathbf{q}) = \sum_{j=1}^{atom} f_j \exp(i\mathbf{r}_j \cdot \mathbf{q}) \qquad (2)$$

where f_j is the atomic scattering factor of the *j*-th atom obtained from the Cromer–Mann formula:

$$f(\sin\theta/\ell) = \sum_{i=1}^{4} a_i \exp[-b_i(\sin\theta/\ell)^2] + c \qquad (3)$$

where ℓ is the radiation wavelength, and the required nine (a_i, b_i, c, i = 1–4) parameters can be found in the literature [74]. Finally, the scattering intensity *I(q)* can be calculated from the structure factor and the polarization factor *P*:

$$I(q) = \left|\mathbf{F}(q)\right|^2 P \qquad (4)$$

$$P = 0.5\left[1 + \cos^2(2\theta)\right] \qquad (5)$$

2.2.4 Diffusion coefficient

The diffusion coefficient, D, of the water molecules (D_W) and hydronium ions (D_H) were calculated using the mean square displacement:

$$D = \lim_{t\to\infty} \frac{1}{6t} \left\langle \left| r(t) - r(0) \right|^2 \right\rangle, \qquad (6)$$

where $r(t)$ is the center-of-mass position vector of the water or the hydronium ion at time t.

3. RESULTS AND DISCUSSION

3.1. Morphologies of the hydrated membranes

3.1.1 Effect of water content on the morphology of the membrane

The isosurface representation of the aqueous domain, including water molecules and sulfonate groups of the polymer, for the PFSA membranes with different SC lengths was plotted to describe the morphology of the water cluster, as shown in Fig. 2. The isosurface representation of the aqueous domain was generated as a volumetric Gaussian density map using the VMD package with a spatial resolution of 1.3 [75, 76]. At λ = 3, the water/sulfonate group domains are distributed over the simulation box and seem to form a channel-network structure. With increasing water content, the water domain gradually increases in size and surrounds the polymer regions (shown as cavity in Fig. 2). At a high water content (e.g. λ = 20), the water domains appear to form a tortuous layered structure in the SSC PFSA membrane but a swollen network structure in the LSC PFSA membrane.

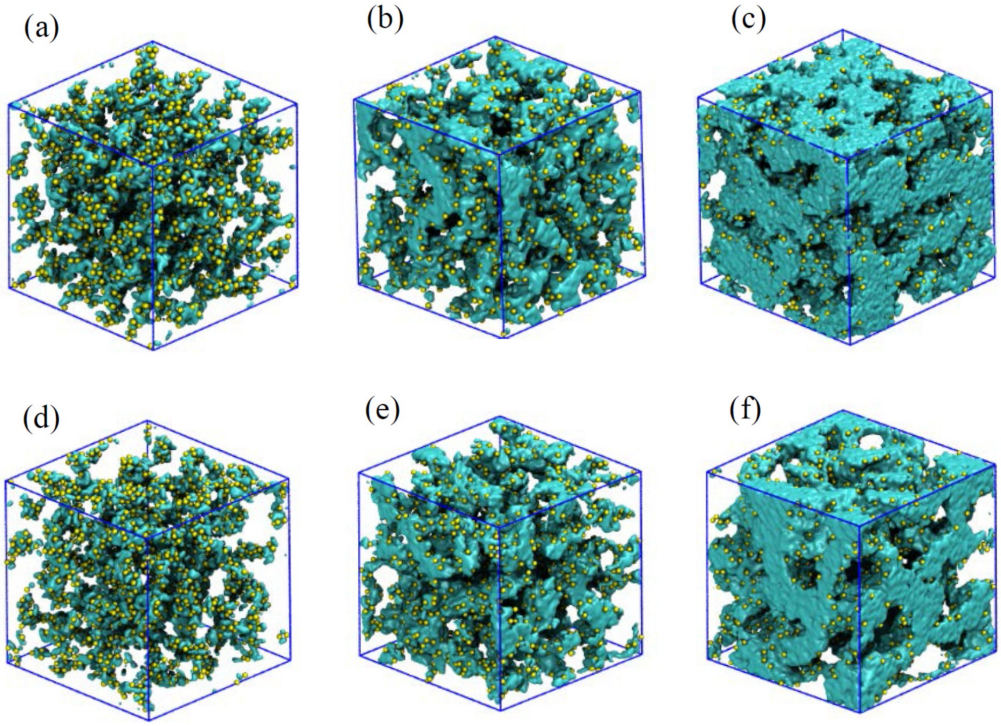

Figure 2. Isosurface representations of water domains including sulfonate groups for SSC (upper panels) and LSC (lower panels) PFSA membranes; (a, d): $\lambda = 3$, (b, e): $\lambda = 9$, and (c, f): $\lambda = 20$. The water region is drawn as a cyan solid contour, and sulfur atoms are represented as yellow particles.

To quantitatively describe the variation in morphology of the PFSA membranes, the ratio of the interfacial area (SA) at the water-polymer boundary to the total volume (TV) of the membrane was calculated and plotted in Fig. 3. For every system, it is found that the SA/TV ratio of each system rapidly increases with increasing water content in the range of λ t 9, while changing only slightly at $\lambda > 9$. The rapid increase in the SA/TV ratio with increasing hydration levels from $\lambda = 3$–9 is due to an increase in the number of water molecules in the

membrane, causing a more pronounced change in the interfacial area at the water-polymer boundary than in the total volume. At high water contents, a lack of significant change in the SA/TV ratio may imply that the increased number of water molecules causes an increase of the water cluster width rather than dispersion of water clusters in the membranes.

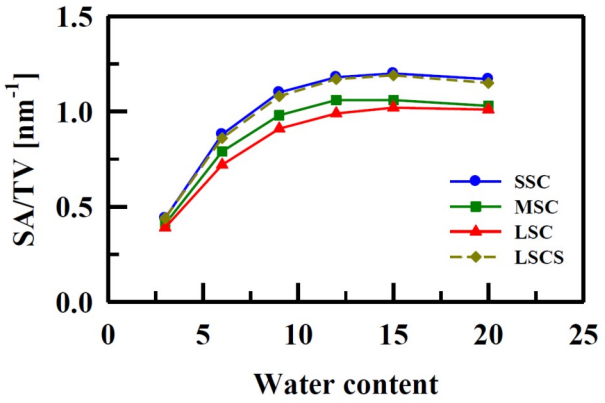

Figure 3. SA/TV ratio of PFSA membranes as a function of water content.

The structure factors, S(q), of the hydrated PFSA membranes were calculated to probe the morphology of the water cluster. The characteristic ionomer peaks of the PFSA membranes at q = ~2 nm^{-1} are shown in Fig. 4 and the corresponding mean cluster separations calculated as $2\pi/q$ are summarized in Table 2. The results clearly show that, with increasing water content, the ionomer peak position of each system shifts to smaller q values and thus the corresponding mean cluster separation increases. The mean cluster separations of the PFSA membranes in the range of 2 to 7 nm are in good agreement with the experimental data of 2.7–6.0 nm [8], except for the membranes with λ = 20.

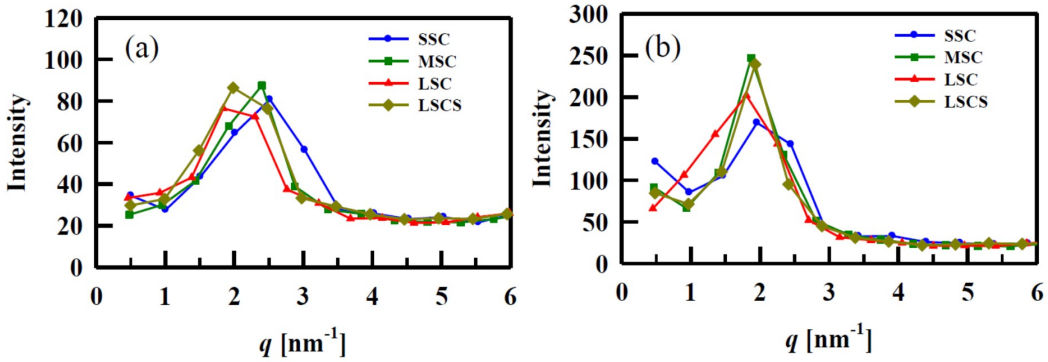

Figure 4. Structure factor of PFSA membranes for which (a) $\lambda = 6$ and (b) $\lambda = 9$. The value of q ranges from 0 to 6.

Table 2. Cluster separation (nm) in PFSA membranes; OW denotes oxygen atoms in water molecules or hydronium ions.

	Group	λ=3	λ=6	λ=9	λ=12	λ=15	λ=20
SSC	Total	2.02	2.50	3.21	3.30	4.51	7.02
	OW	2.43	2.50	3.21	3.30	4.51	7.02
	S	2.02	2.50	2.57	2.64	2.70	2.34
MSC	Total	2.56	2.62	3.36	3.44	4.68	4.84
	OW	2.56	2.62	3.36	3.44	3.51	4.84
	S	2.56	2.62	3.36	3.44	2.81	2.91
LSC	Total	2.67	3.41	3.49	4.75	4.84	7.49
	OW	2.67	3.41	3.49	4.75	4.84	7.49
	S	2.67	2.73	2.79	3.56	2.91	3.75
LSCS	Total	2.06	3.17	3.26	3.34	4.56	4.73
	OW	2.47	2.53	3.26	3.34	4.56	4.73
	S	2.47	2.53	3.26	2.67	2.74	2.84

The partial structure factor for sulfur (S) and oxygen (OW) atoms in a water molecule or hydronium ion, and corresponding mean cluster separation of the S and OW species were also computed (Table 2). It was found that the mean cluster separation of the sulfur cluster (d_S) is smaller than that of the water cluster (d_{OW}) for each PFSA system for which λ >12, with this difference increasing with the water content. This observation is consistent with the results of the analysis of the SA/TV ratio in Fig. 3. Since the sulfonate groups are located at the interface between the polymer and aqueous regions, the increase in the difference between d_S and d_{OW} has been ascribed to the water-layer structure of the aqueous domain in the Nafion membrane [8, 34].

To discuss the difference in the morphologies of the aqueous phases of the SSC and LSC membranes, we computed two-dimensional (2D) number-density plots of the aqueous region, which includes water molecules and sulfonate groups in the PFSA membranes, by using the Gromacs analysis tool (gmx densmap) with a slice thickness of 2 nm, as shown in Fig. 5. At λ = 9, the water and sulfonate groups of SSC PFSA were found to form random water channels, while those of LSC PFSA have a tendency to form local aggregations. The similar results are also observed in the isosurface representations of water domains including sulfonate groups (Fig. 2(b,e)). This implies that the longer SC PFSA membrane possesses more heterogeneous water domains.

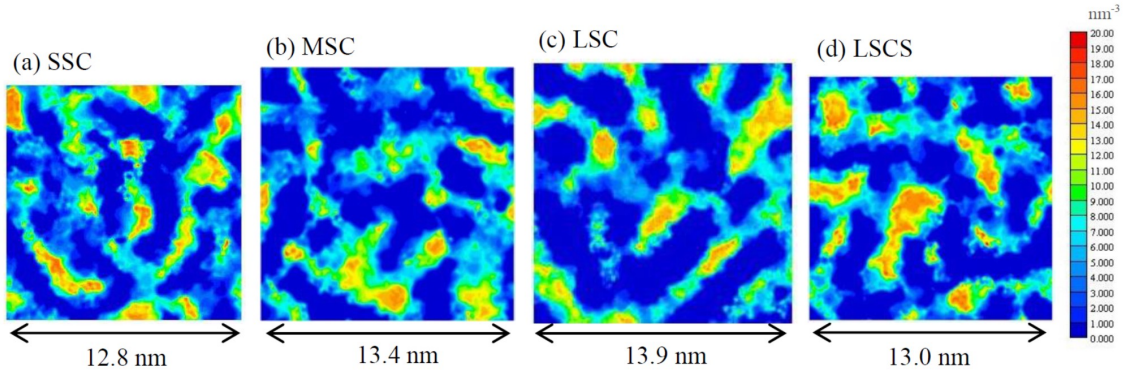

Figure 5. 2D number-density plots of a water region including sulfonate groups in the PFSA membrane with $\lambda = 9$: (a) SSC, (b) MSC, (c) LSC, and (d) LSCS. Color bar indicates number density per nm^3.

The SA/TV ratio (Fig. 3) can be used to quantitatively describe the difference in the morphology of the PFSA membranes with different SC lengths. For a given water content and length of the PTFE backbone (the *x* value in Table 1), a reduction in the SA/TV ratio with increasing PFSA SC length is observed in Fig. 3. A lower SA/TV ratio is indicative of a higher tendency of water to aggregate in a cluster rather than disperse in the membrane. Therefore, this indicates that water tends to be dispersed in the shorter SC PFSA membrane and aggregated in clusters in the longer SC PFSA membrane, which corresponds with the observation in the 2D density-number plots shown in Fig. 5.

The radial distribution functions (RDFs) of S-S and OW-OW for the PFSA membranes are shown in Figs. 6 and S1. The heights of the first peaks for both S-S and OW-OW RDFs increase with increasing PFSA SC length, indicating that the sulfur and water aggregate more in the longer SC PFSA membranes. In addition, the analysis of the structure factors for the membranes at the same hydration level reveals that the mean cluster spacing increases with

increasing SC length (Table 2). This also reflects the fact that the larger water cluster is formed in the longer SC PFSA membrane. The sulfonate group in the LSC PFSA polymer can be extended far from the main chain, contributing to a high probability for interaction with neighboring sulfonate groups and hydronium ions and causing the formation of larger water aggregates in the LSC PFSA membranes. The water and sulfonate groups of the LSC PFSA thus tend to aggregate into a swollen network rather than disperse throughout the membrane as a tortuous layer structure. As a result, as the content increases, the morphology of the hydrophilic cluster changes from a channel network to a tortuous layered structure in the shorter SC PFSA membrane, while the water channel expands to a swollen network in the longer SC PFSA membrane as shown in Scheme 1.

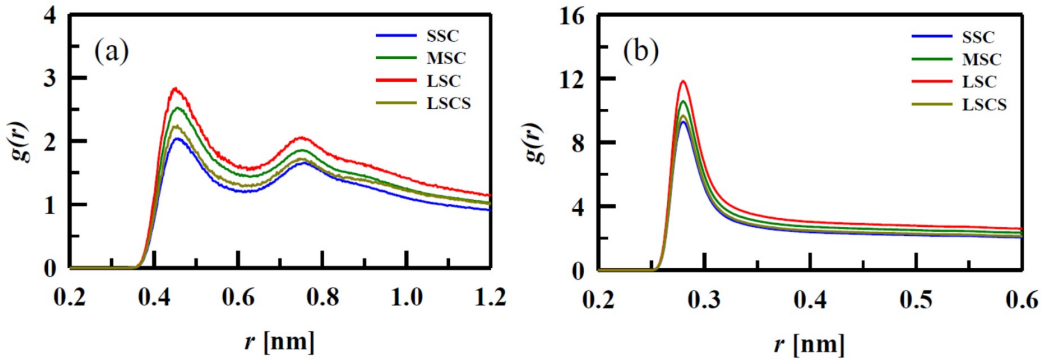

Figure 6. (a) S-S and (b) OW-OW RDF for PFSA membranes for which $\lambda = 9$.

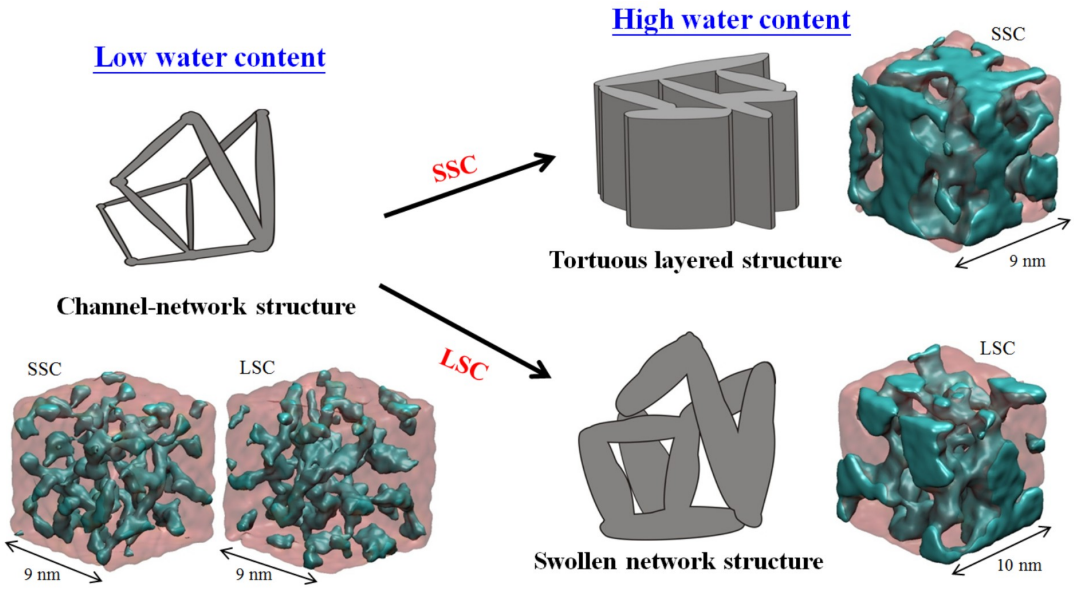

Scheme 1. Schematic illustrating the morphology of the aqueous domains at low and high water contents. The images are extracted from the MD trajectory for the SSC and LSC PFSA membranes. The water and polymer are represented as cyan and pink solid contours, respectively.

Noted that any change in the side chain length while the PTFE backbone length remains constant inevitably results in a change in the value of *EW*. The formation of the larger water cluster in the longer SC PFSA membrane may imply that a PFSA membrane with a higher *EW* increases the size of the water cluster. A similar result was obtained in a previous study which determined that an increase in the PTFE backbone length per sulfonate group, while the side chain length remained constant, also increased the size of the water cluster [34]. These results clearly demonstrated that a PFSA membrane with a higher *EW,* regardless of whether the SC or PTFE backbone of PFSA is longer, tends to exhibit larger aqueous clusters.

In an attempt to determine whether the SC length or the PTFE backbone length per sulfonate group dominates the morphology of a PFSA membrane for which *EW* remains constant, we further compared the structural properties of SSC (x = 7, m = 0) and LSCS (x =

4, m = 2) PFSA membranes, with similar EWs ($EW \approx 1000$). Although analyses of the SA/TV ratio and structure factor showed similar results for the SSC and LSCS PFSA membranes (Figs. 3, 4), the higher peaks of the both S-S and OW-OW RDFs were observed in the LSCS PFSA membrane (Fig. 6), pointing to the presence of more pronounced sulfur and water aggregates in the LSCS PFSA membranes. In addition, the 2D number-density plots for the aqueous region shown in Fig. 5 indicate that the water and sulfonate groups of the LSCS PFSA tend to form larger aqueous clusters rather than random water channels. These results suggest that the SC length dominates the variation in the morphology of the PFSA membrane for a given EW.

In summary, according to a variety of morphological analyses, such as isosurface visualization, surface area, structure factor, number-density map and radial distribution function, we can confirm the following remarks. First, when the water content is increased, the hydrophilic clusters cause the morphology to change from a channel network to a tortuous layered structure in the shorter SC PFSA membrane, while the water swells the channel network structure (rather than form a layered structure) in the longer SC PFSA membrane. Secondly, longer SC PFSA membrane possesses larger and more heterogeneous aqueous clusters owing to more dynamic nature of the chain due to additional ether oxygen. The SC length of the PFSA has a greater influence on the morphology than the PTFE backbone length per sulfonate group, provided the EW value of the PFSA is the same.

3.2. Dynamics of water molecules and hydronium ions

The diffusion coefficients of the water molecules (D_W) and hydronium ions (D_H) in the PFSA membranes are plotted as a function of the water content in Fig. 7. Given the limitations of the simple model adopted for the hydronium ions, the diffusion coefficient calculated in this study reflects only the simple diffusion of a hydronium ion (vehicle

mechanism) and does not take the proton-hopping mechanism (Grötthuss mechanism) into account. Figure 7 shows that both D_W and D_H in the PFSA membranes increase with the water content. This is due to the growth of continuous aqueous domains with the water content. For any given water content, both D_W and D_H decrease as the SC and PTFE lengths increase, although the differences between D_W and D_H of the SSC and MSC are minor. This indicates that the PSFA with the higher-*EW*, and either a longer SC PFSA or PTFE backbone PFSA, is unfavorable for the transport of water and hydronium ions. Since the PFSA with the higher-*EW* tends to form membranes that separated the water clusters, the localized water aggregates reduce the connectivity of the aqueous domain and thus decrease the diffusivities of the water and hydronium ions in the membranes [29, 34].

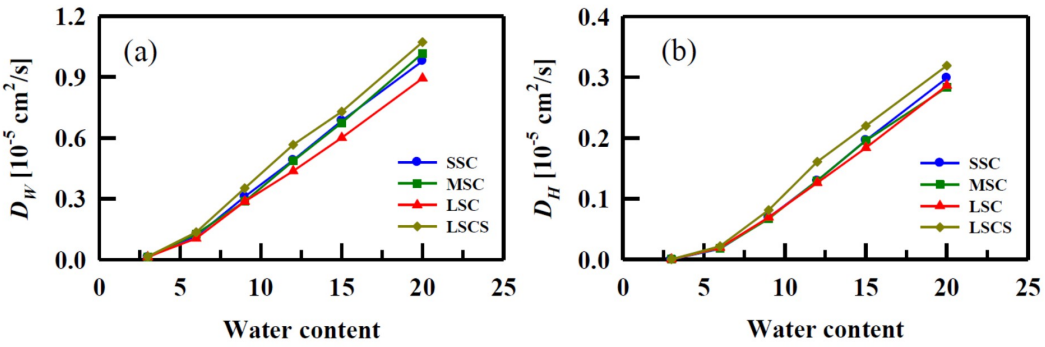

Figure 7. Diffusion coefficients of (a) water molecules and (b) hydronium ions in hydrated PFSA membranes as obtained from MD simulations of medium systems.

Upon comparing the SSC and LSCS PFSA membranes, for which the *EW* values are similar, the values of both D_W and D_H are higher in the LSCS PFSA membranes than in the SSC PFSA membranes. This result was different from our expectations in that localized water clusters in the LSCS PFSA membranes should be unfavorable for water and hydronium ion transport. A possible reason for this is the difference in the size of the aqueous domains of the

SSC and LSCS PFSA membranes. The large aqueous domains of the LSCS PFSA membrane possess more "bulk-like" water, in which the transport of water and hydronium ions is faster. On the other hand, the small aqueous domains of the SSC PFSA membrane are more restrictive of the movement of the water and hydronium ions, leading to comparatively low water and hydronium ion diffusion in the membrane.

3.3. Mechanical deformation of hydrated membranes

The stress-strain (SS) curves of the PFSA membranes were obtained by stretching the membranes along the *z*-axis at a constant strain rate of 0.1 ns^{-1} and a temperature of 300 K. The SS curves can be divided into elastic and plastic regions and provide information including Young's modulus (initial slope at the origin), yield stress, and fracture stress to describe the mechanical properties of the membranes. The SS curves of the PFSA membrane and the corresponding Young's modulus and yield stress are plotted in Figs. 8 and 9, respectively, where Young's modulus is evaluated from the SS curves until strain 0.05 and yield stress is defined as the stress at the 0.2% plastic strain (offset yield point) as shown in the inserted plot of Fig. 8. Noted that simulations of each system were performed three times starting from different initial configurations to examine the dependence of the SS curve on the initial configurations (Fig. S2). No significant difference in the SS curve was observed when the strain was small (< 0.75). The relative error in the Young's modulus and yield stress was found to be < 10% and 5%, respectively. Thus, we confirmed that our simulations could provide meaningful data for discussing the variation in the SS curves for PFSA membranes upon changing the SC lengths and water contents.

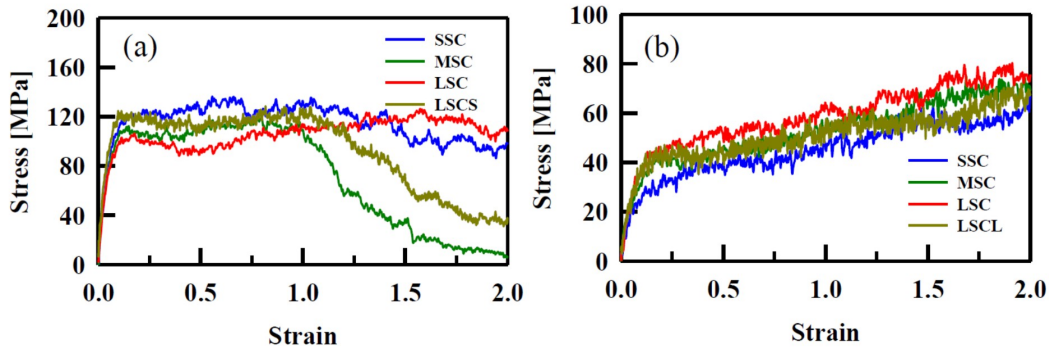

Figure 8. Stress-strain curves for PFSA membranes with (a) λ = 3 and (b) λ = 15 at a strain rate of 0.1 ns^{-1}.

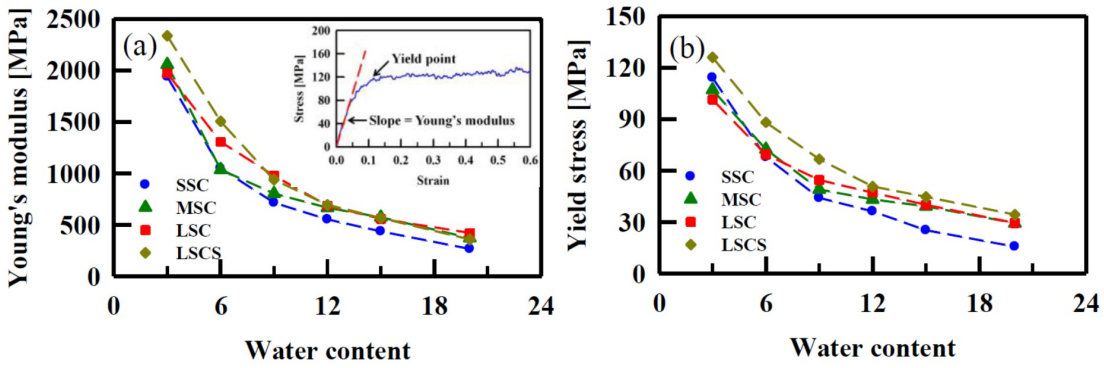

Figure 9. (a) Young's moduli and (b) yield stresses of PFSA membranes as a function of water content measured at a strain rate of 0.1 ns^{-1}.

According to Figures 8 and 9, several intriguing features can be found, even though SS profiles are basically very similar for the three systems. First, at λ = 3, the SS curve of the SSC PFSA membrane shows a small linear-elastic region at strains less than 0.1, followed by the yield point at a strain of ~0.1. Post-yield strain hardening is then observed at greater strains, and fracture occurs at a strain of ~1.0. The SS curves for the MSC, LSC, and LSCS PFSA membranes show slightly different behavior than that for the SSC PFSA membrane. The strain softening is observed in the range of the strain from 0.1 to 0.3, followed by strain hardening. Fracture then occurs at a strain of 1.0−1.5. Secondly, with increasing water content, the yield strain is larger and no fracture is observed up to 200% strain. In addition, both Young's modulus and yield stress decrease as the water content increases. These trends are similar to those observed in experiments [77, 78], even though it is difficult to reproduce the mechanical properties, quantitatively, due to much higher strain rate in our simulations compared with experiments. A more interesting finding is that the effect of the SC length on the mechanical strength of the membrane varies with the water content. Indeed, relative to the SSC PFSA membranes, the LSC PFSA membrane exhibits a lower yield stress when the water content is lower (λ < 6), while a higher yield stress is observed when the water content is higher (λ > 6). In addition, the LSCS PFSA membrane exhibits the highest yield stress among these four PFSA membranes, regardless of the water content. The effects of the SC length and value of *EW* appear to dominate the mechanical strength of the membrane.

In this study, the mechanical properties of the membranes were found to be influenced by the SC length, PTFE backbone length per sulfonic group, and the *EW* value of PFSA. First, as mentioned in Section 3.1, the longer SC PFSA can accommodate larger water clusters. Thus, the polymer domain of the longer SC PFSA also increases in size, which may contribute to the higher modulus. Second, the *EW* value of the PFSA is related to the ionic exchange capacity (*IEC*), defined as $IEC = 1000/EW$. The PFSA with the lower *EW* value and

higher ionic strength may exhibit a higher membrane modulus. Third, the PTFE backbone length per sulfonic group, together with the SC length, may affect the local crystallinity of the membrane and further influence the mechanical strength of the membrane. To clarify the effects of the SC length and PTFE backbone length per sulfonic group on the membrane mechanical strength, the difference in the local crystallinity of these four PFSA membranes was further considered. A characteristic peak of the structure factor for the PFSA membrane at q = ~12 nm^{-1}, which is the overlap of the amorphous and crystalline peaks at q = 11 and 12.4 nm^{-1}, respectively [79], is shown in Fig. 10. The peak is analyzed as the distance between neighboring polymer chains. The corresponding mean chain separations evaluated from the peak positions are given in Table S1. The peak corresponding to the LSCS PFSA membrane is located at the position corresponding to the smallest q value and exhibits the lowest level of crystallinity. It can be assumed that a longer SC PFSA with a shorter PTFE backbone (LSCS) would preferentially form an amorphous structure. Regarding the other three PFSA systems, the peak in the structure factor shifts to the left and becomes broader as the SC length increases at low water contents, but no significant difference in the peak position is observed for high water contents. This indicates that the local crystalline structures decrease and the amorphous structures increase with increasing SC length at low water contents and the difference in the local structure among these three PFSA becomes ambiguous at high water contents. The less local crystalline structure in the longer SC system at low water contents was also observed in the snapshot of the polymer main chain region of the PFSA membrane (Fig. S3).

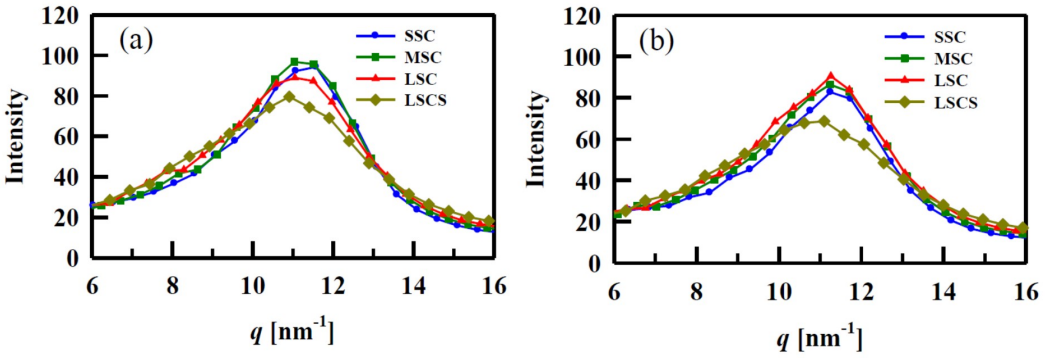

Figure 10. Structure factor of PFSA membranes for which (a) $\lambda = 6$ and (b) $\lambda = 9$ in the range of q from 6 to 16.

Table 3. Comparison of the structure characteristics and yield stress for PFSA membranes.

PFSA	Domain size /SC length	Ionic strength /*EW*	Crystallinity /PTFE backbone length	Yield stress (low λ/high λ)
SSC	Small/short	High/low	High/long	Medium/low
MSC	Medium/medium	Medium/medium	Medium/long	Medium/medium
LSC	Large/long	Low/high	Medium/long	Low/medium
LSCS	Large/long	High/low	Low/short	High/high

Table 3 compares the structure characteristics and yield stresses for all the PFSA models. Among these four PFSA membranes, the LSCS PFSA membrane exhibits the highest yield stress regardless of the water contents but exhibits the lowest level of crystallinity. This indicates that the local crystallinity is not the main factor influencing the mechanical strength of the PFSA membranes. Given the effect of the PTFE backbone length per sulfonic group for a given SC length, the LSCS PFSA with a low *EW* value exhibits a higher yield stress than the LSC PFSA. This is ascribed to the higher ionic strength in the PFSA with a low *EW*

value. Relative to the SSC PFSA, the LSCS PFSA with a similar *EW* value tends to form a larger aggregated structure and thus exhibits a higher mechanical strength. Regarding the effect of the SC length for a given PTFE backbone length, the LSC PFSA with the higher *EW* value exhibits a lower ionic strength and lower crystallinity at a low water content, leading to the low yield stress. However, the difference in the ionic strength and crystallinity between the SSC and LSC becomes ambiguous with an increase in the water content. The LSC PFSA membrane with a large domain size thus exhibits a comparatively higher yield stress for a high water content.

This mechanical simulation successfully explains the effects of the SC length and PTFE backbone length per sulfonic group on the mechanical strength of the PFSA membranes. It is thus possible to say that molecular dynamics simulations can connect microscale morphology and macroscale mechanics and provides great insights to design new materials for PEMFCs.

4. CONCLUSIONS

We carried out a series of MD simulations to determine the effect of pendent SC length on the morphology and mechanical properties of PFSA membranes. The results of simulations demonstrated that the effect of the water content on the morphology is dependent on the SC length. In the PFSA with the shorter SC, the morphology of the aqueous domain changes from a channel-network structure to a tortuous layered structure as the water content increases, while the water swells the channel-network structure rather than forming a water layer in the PFSA membrane with the longer SC. This is due to the more dynamic nature of the long side chain, leading to the formation of larger and more heterogeneous aqueous clusters in a PFSA membrane with a longer SC. The more localized water aggregates in the longer SC PFSA membranes reduce the connectivity of the water network. The diffusivities of the water and hydronium ions are thus lower in those PFSA membranes with the longer SC.

In addition, larger water domains are also observed in the longer-SC PFSA membranes, but with the same *EW*, demonstrating the more pronounced effect of the SC length than the PTFE backbone length on the morphology of the PFSA membrane.

An analysis of the stress-strain curves shows that the LSCS PFSA membrane with least crystallinity exhibits the highest yield stress among the four polymers. This was ascribed to the longer SC and lower *EW* values, contributing to the larger domain size and superior ionic strength. In addition, the LSC PFSA membrane was found to possess a comparatively low mechanical strength at low water contents but a high mechanical strength at high water contents, relative to SSC and MSC PFSA membranes. The LSC PFSA membrane exhibits a comparatively low ionic strength and low crystallinity at low water contents, leading to the low mechanical strength. However, the differences in the ionic strength and crystallinity of the SSC and LSC become minor with an increase in the water content. The LSC PFSA membrane with the large polymer aggregate thus exhibits a comparatively high mechanical strength at high water contents. This study explored the morphological model and explained the effect of SC length on the mechanical properties of PFSA membranes, which will be useful for the design of new materials for fuel cell applications.

5. SUPPORTING INFORMATION

Supplementary material includes radial distribution functions for the PFSA membrane with λ = 3 and 20, stress-strain curves for different initial configurations, the mean chain separation, and snapshots of the polymer main chain region in the PFSA membrane.

6. ACKNOWLEDGMENTS

This research was supported by the Impulsing Paradigm Change through Disruptive Technologies (ImPACT) program. This work was also partially supported by MEXT as a

social and scientific priority issue (“Development of New Fundamental Technologies for High-efficiency Energy Creation, Conversion/Storage, and Use”) to be tackled using the post-K computer. Calculations were performed on the facilities of the supercomputer center at Nagoya University; the Institute for Solid State Physics, the University of Tokyo; Research Center for Computational Science, Okazaki; and, in part, on the K-computer hosted at the RIKEN Advanced Institute for Computational Science (Proposal No. hp150249, hp150275 and hp160247).

7. REFERENCES

[1] K.A. Mauritz, R.B. Moore, State of Understanding of Nafion, Chem. Rev., 104 (2004) 4535-4586.

[2] M. Eikerling, A. Kulikovsky, Polymer Electrolyte Fuel Cells: Physical Principles of Materials and Operation, CRC Press, Boca Raton, FL, 2014.

[3] W.Y. Hsu, T.D. Gierke, Elastic Theory for Ionic Clustering in Perfluorinated Ionomers, Macromolecules, 15 (1982) 101-105.

[4] W.Y. Hsu, T.D. Gierke, Ion Transport and Clustering in Nafion Perfluorinated Membranes, J. Membr. Sci., 13 (1983) 307-326.

[5] L. Rubatat, A.L. Rollet, G. Gebel, O. Diat, Evidence of Elongated Polymeric Aggregates in Nafion, Macromolecules, 35 (2002) 4050-4055.

[6] L. Rubatat, G. Gebel, O. Diat, Fibrillar Structure of Nafion: Matching Fourier and Real Space Studies of Corresponding Films and Solutions, Macromolecules, 37 (2004) 7772-7783.

[7] K. Schmidt-Rohr, Q. Chen, Parallel Cylindrical Water Nanochannels in Nafion Fuel-cell Membranes, Nat. Mater., 7 (2008) 75-83.

[8] K.-D. Kreuer, G. Portale, A Critical Revision of the Nano-Morphology of Proton Conducting Ionomers and Polyelectrolytes for Fuel Cell Applications, Adv. Funct. Mater., 23

(2013) 5390-5397.

[9] K.M. Cable, K.A. Mauritz, R.B. Moore, Anisotropic ionic conductivity in uniaxially oriented perfluorosulfonate ionomers, Chem. Mater., 7 (1995) 1601-1603.

[10] V. Barbi, S.S. Funari, R. Gehrke, N. Scharnagl, N. Stribeck, Nanostructure of Nafion Membrane Material as a Function of Mechanical Load Studied by SAXS, Polymer, 44 (2003) 4853-4861.

[11] D. Liu, M.A. Hickner, S.W. Case, J.J. Lesko, Relaxation of Proton Conductivity and Stress in Proton Exchange Membranes Under Strain, J. Eng. Mater. Technol., 128 (2006) 503-508.

[12] J. Lin, R. Wycisk, P.N. Pintauro, M. Kellner, Stretched Recast Nafion for Direct Methanol Fuel Cells, Electrochem. Solid State Lett., 10 (2007) B19-B22.

[13] J. Li, J.K. Park, R.B. Moore, L.A. Madsen, Linear Coupling of Alignment with Transport in a Polymer Electrolyte Membrane, Nat. Mater., 10 (2011) 507-511.

[14] J.K. Park, J. Li, G.M. Divoux, L.A. Madsen, R.B. Moore, Oriented Morphology and Anisotropic Transport in Uniaxially Stretched Perfluorosulfonate Ionomer Membranes, Macromolecules, 44 (2011) 5701-5710.

[15] H. Mendil-Jakani, S. Pouget, G. Gebel, P.N. Pintauro, Insight into the Multiscale Structure of Pre-stretched Recast Nafion® Membranes: Focus on the Crystallinity Features, Polymer, 63 (2015) 99-107.

[16] S. Paddison, Proton conduction mechanisms at low degrees of hydration in sulfonic acid-based polymer electrolyte membranes, Ann. Rev. Mater. Res., 33 (2003) 289-319.

[17] K.-D. Kreuer, S.J. Paddison, E. Spohr, M. Schuster, Transport in Proton Conductors for Fuel-Cell Applications: Simulations, Elementary Reactions, and Phenomenology, Chem. Rev., 104 (2004) 4637-4678.

[18] J.A. Elliott, S.J. Paddison, Modelling of morphology and proton transport in PFSA

membranes, Phys. Chem. Chem. Phys., 9 (2007) 2602-2618.

[19] S.J. Paddison, J.A. Elliott, Molecular Modeling of the Short-Side-Chain Perfluorosulfonic Acid Membrane, J. Phys. Chem. A, 109 (2005) 7583-7593.

[20] S.J. Paddison, J.A. Elliott, On the consequences of side chain flexibility and backbone conformation on hydration and proton dissociation in perfluorosulfonic acid membranes, Phys. Chem. Chem. Phys., 8 (2006) 2193-2203.

[21] S.S. Jang, V. Molinero, T. Çağın, W.A. Goddard, Nanophase-Segregation and Transport in Nafion 117 from Molecular Dynamics Simulations: Effect of Monomeric Sequence, J. Phys. Chem. B, 108 (2004) 3149-3157.

[22] S. Urata, J. Irisawa, A. Takada, W. Shinoda, S. Tsuzuki, M. Mikami, Molecular Dynamics Simulation of Swollen Membrane of Perfluorinated Ionomer, J. Phys. Chem. B, 109 (2005) 4269-4278.

[23] R. Devanathan, A. Venkatnathan, M. Dupuis, Atomistic Simulation of Nafion Membrane: I. Effect of Hydration on Membrane Nanostructure, J. Phys. Chem. B, 111 (2007) 8069-8079.

[24] R. Devanathan, A. Venkatnathan, M. Dupuis, Atomistic Simulation of Nafion Membrane. 2. Dynamics of Water Molecules and Hydronium Ions, J. Phys. Chem. B, 111 (2007) 13006-13013.

[25] A. Venkatnathan, R. Devanathan, M. Dupuis, Atomistic Simulations of Hydrated Nafion and Temperature Effects on Hydronium Ion Mobility, J. Phys. Chem. B, 111 (2007) 7234-7244.

[26] D. Brandell, J. Karo, A. Liivat, J. Thomas, Molecular Dynamics Studies of the Nafion®, Dow® and Aciplex® Fuel-cell Polymer Membrane Systems, J. Mol. Model., 13 (2007) 1039-1046.

[27] S. Cui, J. Liu, M.E. Selvan, D.J. Keffer, B.J. Edwards, W.V. Steele, A Molecular

Dynamics Study of a Nafion Polyelectrolyte Membrane and the Aqueous Phase Structure for Proton Transport, J. Phys. Chem. B, 111 (2007) 2208-2218.

[28] R. Devanathan, A. Venkatnathan, R. Rousseau, M. Dupuis, T. Frigato, W. Gu, V. Helms, Atomistic Simulation of Water Percolation and Proton Hopping in Nafion Fuel Cell Membrane, J. Phys. Chem. B, 114 (2010) 13681-13690.

[29] J. Liu, N. Suraweera, D.J. Keffer, S. Cui, S.J. Paddison, On the Relationship between Polymer Electrolyte Structure and Hydrated Morphology of Perfluorosulfonic Acid Membranes, J. Phys. Chem. C, 114 (2010) 11279-11292.

[30] A.P. Sunda, A. Venkatnathan, Atomistic simulations of structure and dynamics of hydrated Aciplex polymer electrolyte membrane, Soft Matter, 8 (2012) 10827-10836.

[31] T. Mabuchi, T. Tokumasu, Effect of Bound State of Water on Hydronium Ion Mobility in Hydrated Nafion Using Molecular Dynamics Simulations, J. Chem. Phys., 141 (2014) 104904.

[32] C.K. Knox, G.A. Voth, Probing Selected Morphological Models of Hydrated Nafion Using Large-Scale Molecular Dynamics Simulations, J. Phys. Chem. B, 114 (2010) 3205-3218.

[33] P.V. Komarov, P.G. Khalatur, A.R. Khokhlov, Large-scale Atomistic and Quantum-mechanical Simulations of a Nafion Membrane: Morphology, Proton Solvation and Charge Transport, Beilstein J. Nanotechnol., 4 (2013) 567-587.

[34] A.-T. Kuo, W. Shinoda, S. Okazaki, Molecular Dynamics Study of the Morphology of Hydrated Perfluorosulfonic Acid Polymer Membranes, J. Phys. Chem. C, 120 (2016) 25832-25842.

[35] S. Ban, C. Huang, X.-Z. Yuan, H. Wang, Molecular Simulation of Gas Adsorption, Diffusion, and Permeation in Hydrated Nafion Membranes, J. Phys. Chem. B, 115 (2011) 11352-11358.

[36] K.B. Daly, J.B. Benziger, P.G. Debenedetti, A.Z. Panagiotopoulos, Molecular Dynamics Simulations of Water Sorption in a Perfluorosulfonic Acid Membrane, J. Phys. Chem. B, 117 (2013) 12649-12660.

[37] K.B. Daly, J.B. Benziger, A.Z. Panagiotopoulos, P.G. Debenedetti, Molecular Dynamics Simulations of Water Permeation across Nafion Membrane Interfaces, J. Phys. Chem. B, 118 (2014) 8798-8807.

[38] E. Allahyarov, P.L. Taylor, Simulation Study of the Correlation between Structure and Conductivity in Stretched Nafion, J. Phys. Chem. B, 113 (2009) 610-617.

[39] K. Abu-Hakmeh, P. Sood, B. Jae Chun, J. Choi, S. Jang, Effect of Uniaxial Deformation on Structure and Transport in Hydrated Nafion 117: Molecular Dynamics Simulation Study, Mater. Performance Charact., 4 (2015) 131-147.

[40] M. Ozmaian, R. Naghdabadi, Properties of Nafion Under Uniaxial Loading at Different Temperatures: A Molecular Dynamics Study, Polym. Plast. Technol. Eng., 54 (2015) 806-813.

[41] J. Xie, S. Ban, B. Liu, H. Zhou, A Molecular Simulation Study of Chemical Degradation and Mechanical Deformation of Hydrated Nafion Membranes, Appl. Surf. Sci., 362 (2016) 441-447.

[42] A.-T. Kuo, A. Tanaka, J. Irisawa, W. Shinoda, S. Okazaki, Molecular Dynamics Study on the Mechanical Deformation of Hydrated Perfluorosulfonic Acid Polymer Membranes, J. Phys. Chem. C, 121 (2017) 21374-21382.

[43] M.K. Petersen, G.A. Voth, Characterization of the Solvation and Transport of the Hydrated Proton in the Perfluorosulfonic Acid Membrane Nafion, J. Phys. Chem. B, 110 (2006) 18594-18600.

[44] M.K. Petersen, A.J. Hatt, G.A. Voth, Orientational Dynamics of Water in the Nafion Polymer Electrolyte Membrane and Its Relationship to Proton Transport, J. Phys. Chem. B, 112 (2008) 7754-7761.

[45] S. Feng, G.A. Voth, Proton Solvation and Transport in Hydrated Nafion, J. Phys. Chem. B, 115 (2011) 5903-5912.

[46] S. Feng, J. Savage, G.A. Voth, Effects of Polymer Morphology on Proton Solvation and Transport in Proton-Exchange Membranes, J. Phys. Chem. C, 116 (2012) 19104-19116.

[47] Y.-L.S. Tse, A.M. Herring, K. Kim, G.A. Voth, Molecular Dynamics Simulations of Proton Transport in 3M and Nafion Perfluorosulfonic Acid Membranes, J. Phys. Chem. C, 117 (2013) 8079-8091.

[48] J. Savage, Y.-L.S. Tse, G.A. Voth, Proton Transport Mechanism of Perfluorosulfonic Acid Membranes, J. Phys. Chem. C, 118 (2014) 17436-17445.

[49] J. Savage, G.A. Voth, Proton Solvation and Transport in Realistic Proton Exchange Membrane Morphologies, J. Phys. Chem. C, 120 (2016) 3176-3186.

[50] S. Yamamoto, S.-a. Hyodo, A Computer Simulation Study of the Mesoscopic Structure of the Polyelectrolyte Membrane Nafion, Polym. J., 35 (2003) 519-527.

[51] K. Malek, M. Eikerling, Q. Wang, Z. Liu, S. Otsuka, K. Akizuki, M. Abe, Nanophase segregation and water dynamics in hydrated Nafion: Molecular modeling and experimental validation, J. Chem. Phys., 129 (2008) 204702.

[52] D. Wu, S.J. Paddison, J.A. Elliott, A comparative study of the hydrated morphologies of perfluorosulfonic acid fuel cell membranes with mesoscopic simulations, Energy Environ. Sci., 1 (2008) 284-293.

[53] R. Jorn, G.A. Voth, Mesoscale Simulation of Proton Transport in Proton Exchange Membranes, J. Phys. Chem. C, 116 (2012) 10476-10489.

[54] K. Morohoshi, T. Hayashi, Modeling and Simulation for Fuel Cell Polymer Electrolyte Membrane, Polymers, 5 (2013) 56.

[55] A. Vishnyakov, A.V. Neimark, Self-Assembly in Nafion Membranes upon Hydration: Water Mobility and Adsorption Isotherms, J. Phys. Chem. B, 118 (2014) 11353-11364.

[56] S. Liu, J. Savage, G.A. Voth, Mesoscale Study of Proton Transport in Proton Exchange Membranes: Role of Morphology, J. Phys. Chem. C, 119 (2015) 1753-1762.

[57] M. Ghelichi, K. Malek, M.H. Eikerling, Ionomer Self-Assembly in Dilute Solution Studied by Coarse-Grained Molecular Dynamics, Macromolecules, 49 (2016) 1479-1489.

[58] A.-T. Kuo, S. Okazaki, W. Shinoda, Transferable coarse-grained model for perfluorosulfonic acid polymer membranes, J. Chem. Phys., 147 (2017) 094904.

[59] K. Prater, The renaissance of the solid polymer fuel cell, J. Power Sources, 29 (1990) 239-250.

[60] J. Halim, F.N. Büchi, O. Haas, M. Stamm, G.G. Scherer, Characterization of perfluorosulfonic acid membranes by conductivity measurements and small-angle x-ray scattering, Electrochim. Acta, 39 (1994) 1303-1307.

[61] C.A. Edmondson, P.E. Stallworth, M.E. Chapman, J.J. Fontanella, M.C. Wintersgill, S.H. Chung, S.G. Greenbaum, Complex impedance studies of proton-conducting membranes, Solid State Ion., 135 (2000) 419-423.

[62] A. Stassi, I. Gatto, E. Passalacqua, V. Antonucci, A.S. Arico, L. Merlo, C. Oldani, E. Pagano, Performance comparison of long and short-side chain perfluorosulfonic membranes for high temperature polymer electrolyte membrane fuel cell operation, J. Power Sources, 196 (2011) 8925-8930.

[63] S. Cui, J. Liu, M.E. Selvan, S.J. Paddison, D.J. Keffer, B.J. Edwards, Comparison of the Hydration and Diffusion of Protons in Perfluorosulfonic Acid Membranes with Molecular Dynamics Simulations, J. Phys. Chem. B, 112 (2008) 13273-13284.

[64] A.P. Sunda, A. Venkatnathan, Molecular dynamics simulations of side chain pendants of perfluorosulfonic acid polymer electrolyte membranes, J. Mater. Chem. A, 1 (2013) 557-569.

[65] L. Martinez, R. Andrade, E.G. Birgin, J.M. Martinez, PACKMOL: A Package for Building Initial Configurations for Molecular Dynamics Simulations, J. Comput. Chem., 30

(2009) 2157-2164.

[66] S. Pronk, S. Páll, R. Schulz, P. Larsson, P. Bjelkmar, R. Apostolov, M.R. Shirts, J.C. Smith, P.M. Kasson, D. van der Spoel, B. Hess, E. Lindahl, GROMACS 4.5: A High-Throughput and Highly Parallel Open Source Molecular Simulation Toolkit, Bioinformatics, 29 (2013) 845-854.

[67] M.J. Abraham, T. Murtola, R. Schulz, S. Páll, J.C. Smith, B. Hess, E. Lindahl, GROMACS: High Performance Molecular Simulations Through Multi-Level Parallelism From Laptops to Supercomputers, SoftwareX, 1–2 (2015) 19-25.

[68] M. Levitt, M. Hirshberg, R. Sharon, K.E. Laidig, V. Daggett, Calibration and Testing of a Water Model for Simulation of the Molecular Dynamics of Proteins and Nucleic Acids in Solution, J. Phys. Chem. B, 101 (1997) 5051-5061.

[69] G.J. Martyna, M.L. Klein, M. Tuckerman, Nose-Hoover Chains: The Canonical Ensemble via Continuous Dynamics J. Chem. Phys., 97 (1992) 2635-2643.

[70] M. Parrinello, A. Rahman, Polymorphic Transitions in Single Crystals: A New Molecular Dynamics Method, J. Appl. Phys., 52 (1981) 7182-7190.

[71] G.J. Martyna, D.J. Tobias, M.L. Klein, Constant Pressure Molecular Dynamics Algorithms, J. Chem. Phys., 101 (1994) 4177-4189.

[72] U. Essmann, L. Perera, M.L. Berkowitz, T. Darden, H. Lee, L.G. Pedersen, A smooth particle mesh Ewald method, J. Chem. Phys., 103 (1995) 8577-8593.

[73] F. Eisenhaber, P. Lijnzaad, P. Argos, C. Sander, M. Scharf, The double cubic lattice method: Efficient approaches to numerical integration of surface area and volume and to dot surface contouring of molecular assemblies, J. Comput. Chem., 16 (1995) 273-284.

[74] D.T. Cromer, J.B. Mann, X-ray Scattering Factors Computed from Numerical Hartree-Fock Wave Functions, Acta Crystall. A, 24 (1968) 321-324.

[75] W. Humphrey, A. Dalke, K. Schulten, VMD: Visual molecular dynamics, J. Mol.

Graphics, 14 (1996) 33-38.

[76] M. Krone, J.E. Stone, T. Ertl, K. Schulten, Fast visualization of gaussian density surfaces for molecular dynamics and particle system trajectories, EuroVis-Short Papers, 1 (2012) 67-71.

[77] M.N. Silberstein, M.C. Boyce, Constitutive Modeling of the Rate, Temperature, and Hydration Dependent Deformation Response of Nafion to Monotonic and Cyclic Loading, J. Power Sources, 195 (2010) 5692-5706.

[78] Z. Lu, M. Lugo, M.H. Santare, A.M. Karlsson, F.C. Busby, P. Walsh, An Experimental Investigation of Strain Rate, Temperature and Humidity Effects on the Mechanical Behavior of a Perfluorosulfonic Acid Membrane, J. Power Sources, 214 (2012) 130-136.

[79] P.C. van der Heijden, L. Rubatat, O. Diat, Orientation of Drawn Nafion at Molecular and Mesoscopic Scales, Macromolecules, 37 (2004) 5327-5336.